# Accepted Manuscript


Title: Hydrophobic Residues at Position 10 of α-Conotoxin PnIA Influence Subtype Selectivity between α7 and α3β2 Neuronal Nicotinic Acetylcholine Receptors

Author: Gene Hopping Ching-I Anderson Wang Ron C. Hogg Simon T. Nevin Richard J. Lewis David J. Adams Paul F. Alewood

PII: S0006-2952(14)00446-8
DOI: http://dx.doi.org/doi:10.1016/j.bcp.2014.07.025
Reference: BCP 12041

To appear in: *BCP*

Received date: 10-4-2014
Revised date: 25-7-2014
Accepted date: 28-7-2014

Please cite this article as: Hopping G, Wang C-IA, Hogg RC, Nevin ST, Lewis RJ, Adams DJ, Alewood PF, Hydrophobic Residues at Position 10 of *rmalpha*-Conotoxin PnIA Influence Subtype Selectivity between *rmalpha*7 and *rmalpha*3*rmbeta*2 Neuronal Nicotinic Acetylcholine Receptors, *Biochemical Pharmacology* (2014), http://dx.doi.org/10.1016/j.bcp.2014.07.025

**24 July 2014**

**Biochem. Pharmacol.**

# Hydrophobic Residues at Position 10 of α-Conotoxin PnIA Influence Subtype Selectivity between α7 and α3β2 Neuronal Nicotinic Acetylcholine Receptors

Gene Hopping[a], Ching-I Anderson Wang[a], Ron C. Hogg[b], Simon T. Nevin[c], Richard J. Lewis[a], David J. Adams[c,d], and Paul F. Alewood[a,*]

[a]Institute for Molecular Bioscience, The University of Queensland, St Lucia, Queensland 4072, Australia.

[b]Department of Neuroscience, Centre Medical Universitaire, Medical Faculty, 1 rue Michel Servet, CH-1211 Geneva 4, Switzerland.

[c]Queensland Brain Institute, The University of Queensland, St Lucia, Queensland 4072, Australia.

[d]Health Innovations Research Institute, RMIT University, Bundoora, Victoria 3083, Australia.

*Author to whom correspondence should be addressed.

Abbreviations used: nAChR, nicotinic acetylcholine receptor; α-Ctx, α-conotoxin; AChBP, acetylcholine binding protein; Abu, aminobuteric acid; Nva, norvaline; Nle, norleucine; Aha,

aminoheptanoic acid; Aoa, aminooctanoic acid; Cha, cyclohexylalanine; Nal, naphthylalanine; Boc, benzyloxycarbonyl; Bzl, benzyl.

**Abstract**

Neuronal nicotinic acetylcholine receptors (nAChRs) are a diverse class of ligand-gated ion channels involved in neurological conditions such as neuropathic pain and Alzheimer's disease. α-Conotoxin [A10L]PnIA is a potent and selective antagonist of the mammalian α7 nAChR with a key binding interaction at position 10. We now describe a molecular analysis of the receptor – ligand interactions that determine the role of position 10 in determining potency and selectivity for the α7 and α3β2 nAChR subtypes. Using electrophysiological and radioligand binding methods on a suite of [A10L]PnIA analogs we observed that hydrophobic residues in position 10 maintained potency at both subtypes whereas charged or polar residues abolished α7 binding. Molecular docking revealed dominant hydrophobic interactions with several α7 and α3β2 receptor residues via a hydrophobic funnel. Incorporation of norleucine (Nle) caused the largest (8-fold) increase in affinity for the α7 subtype (Ki = 44 nM) though selectivity reverted to α3β2 ($IC_{50}$ = 0.7 nM). It appears that that placement of a single methyl group determines selectivity between α7 and α3β2 nAChRs via different molecular determinants.

## 1. Introduction

Nicotinic acetylcholine receptors (nAChRs), along with $GABA_A$ [1], 5-$HT_3$ [2] and glycine receptors, are members of the Cys-loop ligand-gated ion channel superfamily [3]. Structurally, nAChRs are pentamers, consisting of 5 subunits that each contain an N-terminal extracellular domain (ligand-binding domain), a transmembrane domain containing four transmembrane helices, and an intracellular domain [4,5]. These subunits associate to form a central, solvated, cation-conducting pore [6]. Neuronal nAChRs consist of either homomeric α subunits (α7, α8 or α9) or a combination of α and β subunits. This diverse subunit combination creates receptors with distinct pharmacological properties [7].

Neuronal nAChRs have been implicated in a variety of disease states, including Alzheimer's disease [8], schizophrenia [9], a genetically transmissible form of epilepsy [10], inflammation and pain [11], and the autoimmune disease myasthenia gravis [12]. As such, there is great interest in characterizing ligands that can discriminate between different subunit arrangements of this receptor.

Conotoxins are a diverse group of disulfide-rich peptides with exquisite selectivity for many mammalian ion channel and receptor subtypes [13-16]. α-Conotoxins (α-Ctxs) range in size from 9−14 amino acids and have an affinity for a variety of nAChR subtypes. Their small size, rigid framework consisting of four- and seven-residue loops conferred by two disulfide bonds, and ease of synthesis make them ideal for structure−function studies **(Table 1)** [17-19].

We and others have previously reported that a single amino acid change at position 10 between two closely related α-Ctxs, PnIA and PnIB, caused nAChR subtype selectivity to change from the α3β2 to α7 [20-22]. In further studies, α-Ctx [A10L]PnIA, acted as an antagonist of chick

wild-type α7 nAChRs expressed in *Xenopus* oocytes, as well as being an α7-L247T receptor agonist [23]. The α7-L247T receptor renders the closed state of the receptor conductive, and can be used to probe ligand interactions with otherwise electropharmacologically silent states. This highlights the ability of selective ligands to dissect the structure-function of these receptors. Computational docking studies [24] and crystal structures of conotoxin analogues bound to the analogous acetylcholine binding protein (AChBP) have revealed how the toxins and receptors interact, including how the residue at position 10 interacts with the (+)-face of the β subunit [25-30].

To explore in more detail the nature of the intermolecular interactions of α-Ctx [A10L]PnIA that control selectivity between the α7 and α3β2 nAChRs, we used a chemical peptide synthesis strategy to evaluate a range of coded and non-coded amino acids in position 10 that vary in polarity, shape and size **(Figure 1)**. The strategy employed was to select the tightest binding analogues at the α7 nAChR and evaluate their functional activity in α7, α3β2 and α4β2 nAChR assays to determine the position 10 influence on nicotinic receptor subtype selectivity.

## 2. Materials and Methods

All Boc-amino acids (with the exception of Boc-aminoheptanoic acid and Boc-aminooctanoic acid) and 2-(1*H*-benzotriazol-1-yl)-1,1,3,3-tetramethyl uronium hexafluorophosphate (HBTU) were from NovaBiochem (San Diego, CA). diethylisopropylamine (DIEA) and dimethylformamide (DMF) were purchased from Auspep (Melbourne, Australia). 4-methylbenzylhydrylamine resin was purchased from Peptide Institute (Osaka, Japan). *P*-cresol, *p*-thiocresol were from Sigma-Aldrich (Sydney, Australia). Anhydrous hydrogen fluoride was from

Boc Gasses (Sydney, Australia). HPLC grade acetonitrile (Lab Scan, Bangkok, Thailand) and distilled $H_2O$ (ELGA, Melbourne, Australia) were used throughout this work. All other organic reagents and solvents, unless stated otherwise, were purchased from Sigma-Aldrich (Sydney, Australia).

**2.1 Synthesis of 2-*tert*-Butyloxycarbonylaminoheptanoic acid**

The aliphatic amino acids were synthesized as described previously [31]. Diethyl acetamidomalonate (15 g, 69 mmol) and 1-bromopentane (12 mL, 97 mmol) were heated at reflux in a solution of sodium (1.9 g, 83 mmol) in ethanol (50 mL) for 24 h. Upon cooling, the reaction mixture was poured onto crushed ice (300 mL) and the precipitate was filtered and washed with water. The resulting solid was placed in a 500 mL round-bottom flask to which concentrated HCl (90 mL) and dimethylformamide (10 mL) were added. The mixture was heated at reflux overnight. After cooling, nitrogen was bubbled through the solution for 3 h to reduce the concentration of HCl. The reaction mixture was then diluted 2-fold with 50% ethanol (aq), which we had increased the pH to 5 through adding KOH(s). At this pH a precipitate began to form, and the solution was kept at 4$^{o}$C overnight. The precipitate was collected, washed with ice cold ethanol, and air dried to afford 3.8 g, of white, needle-like crystals. The crystals (3.8 g, 26 mmol) and potassium carbonate (7.2 g, 52 mmol) were dissolved in water (30 mL). To this solution, di-*tert*-butyldicarbonate (6.86 g, 31.4 mmol) dissolved in tetrahydrofuran (50 mL) was slowly added. The solution was then stirred vigorously for 3 h. Water (50 mL) and diethyl ether (50 mL) were added, and the aqueous layer collected and further extracted with ether (50 mL). The aqueous layer was then acidified to pH 2 with citric acid (50% solution w/v). The resulting precipitate was extracted with ethyl acetate (2 x 50 mL) and dried over magnesium sulfate before the solvent was removed under reduced pressure. The resulting oil was stored at 4$^{o}$C overnight

and an amorphous solid formed. The product was recrystallized from ethyl acetate/hexane yielding 4.4 g, 70% of a white solid. $^{1}$H NMR (DMSO-d6, 300 MHz) δ 0.96 (t, J=6.2 Hz, 3H), 1.20 (m, 6H), 1.38 (s, 9H), 1.58 (m, 2H), 1.62 (m, 2H), 3.60 (m, 1H), 7.5 (d, J=9.0 Hz, 1H); HRMS [obs. M+H$^{+}$ 245.1426 Da; calc. 245.1627 Da].

**2.2 Synthesis of 2-*tert*-butyloxycarbonylaminooctanoic acid**

This synthesis used the same method used for Aha, with1-bromopentane being used instead of 1-bromohexane. The yield of 2-aminooctanoic acid was 54%, whereas the yield of the title compound was 67%, and isolated as an amorphous white solid. $^{1}$H NMR (DMSO-d6, 300 MHz) δ 0.85 (t, J=7.2 Hz, 3H), 1.23 (m, 8H), 1.38 (s, 9H), 1.55 (m, 2H), 1.60 (m, 2H), 3.88 (m, 1H), 7.2 (d, J=9.1 Hz, 1H); HRMS [obs. M+H$^{+}$ 259.1777 Da; calc. 259.1784 Da].

**2.3 Peptide synthesis**

Peptides were synthesized manually on a 0.5 mM scale using Boc/Bzl chemistry with *in situ* neutralization protocols [32]. Amino acids were incorporated with the following side chain protecting groups: Cys(Meb), Asp(OcHex), Glu(OcHex), Lys(2-ClZ), Asn(Xan), Gln(Xan), Arg(Tos), Ser(Bzl), Thr(Bzl), Trp(For) and Tyr(2-BrZ). All other amino acids were incorporated unprotected.

Deprotection of the N-terminal Boc group was afforded using neat trifluoroacetic acid (TFA; 2 x 1 min), followed by a 1 min DMF flow wash. The amino acid (2 mmol) was dissolved in a 0.5 mM solution of HBTU in DMF (4 mL). DIEA (460 μL, 2.6 mmol) was added to the amino acid solution immediately before the drained resin was added. The amino acid was allowed to couple for 10 min, whereby a ninhydrin reaction was performed. If the coupling was 99.6% complete or more, the coupling solution was drained, resin washed with DMF, and the Boc group removed

with TFA treatment (2 x 1 min). If the coupling was less than 99.6%, the coupling solution was drained, the resin washed with DMF and a fresh solution of activated amino acid was re-coupled. If coupling was less than 99.6 % after 2 coupling rounds, the free amino groups were acetylated.

Residues 11−16 were manually assembled in one large batch on 4-methylbenzhydrylamine resin **(Figure 2)**. After addition of asparagine 11 to the growing peptide chain, the resin was washed and dried. The large batch was then split 17 ways to provide the base sequence for all analogues (PnIA, [A10L]PnIA and 15 analogues). All peptides assembled smoothly, with average coupling efficiencies of 99.96% as determined by the quantitative ninhydrin assay [33].

Resin (300 mg) was cleaved in 10 mL of anhydrous HF, in the presence of p-cresol and p-thiocresol (18:1:1 HF:p-cresol:p-thiocresol). The reaction was carried out at 0$^{o}$C for 1.5 h. The HF was removed under vacuum and deprotected peptides precipitated by adding ice cold diethyether. The solution was filtered through a polypropylene filter and the peptides were dissolved away from the resin by adding a 45% solution of acetonitrile in 0.1% TFA (aq) before lyophilization. Peptides were identified by analytical HPLC and mass spectrometric (MS) analysis, and purified further by preparative HPLC, if necessary. Oxidative folding was achieved by diluting peptides to 0.1 mg/mL in a 30% isopropanol/0.1 M ammonium bicarbonate solution, pH 8, in an open vessel and stirring. It was previously demonstrated that adding a water-miscible organic solvent promotes the formation of the desired native (globular (1−3, 2−4)) disulfide arrangement [21,34-36] with increased HPLC retention times indicating that the oxidized folded product was more hydrophobic than its reduced precursor. Presence of fully oxidized material was determined when MS analysis showed a loss of 4 amu. The oxidation solution was acidified to pH 2 with neat TFA and the volume of solution reduced at the rotary evaporator. The concentrated oxidized solution was then diluted with 0.05% TFA (aq) before being filtered

through a 0.45 μM disposable syringe filter. The major product was isolated by preparative HPLC and lyophilized. We synthesized all analogues in 20–30% yield of the peptides based on the initial resin loading.

**2.4 HPLC and MS Analysis**

Analytical HPLC was performed on a Shimadzu LC-2010a HPLC equipped with a dual wavelength UV detector monitoring at 214 nm and 280 nm, using a Vydac C18 250 mm x 4.6 mm ID, 300 Å column, operating at a flow rate of 1 mL/min. A routine solvent gradient of 0–40% buffer B (0.043% TFA in 90% $CH_3CN$ (aq)) in buffer A (0.05 % TFA (aq)) over 40 min was used. Preparative HPLC were performed using a Waters 600E solvent delivery system fitted with a 484 UV absorbance detector, using a Phenomenex Jupiter C18 250 mm x 21.2 mm ID 300 Å column, operating at a flow rate of 10 mL/min. Absorbance was monitored at 230 nm. Fractions were taken manually, and analyzed by ESI-MS and analytical HPLC.

Mass spectra were acquired using an LCT-TOF mass spectrometer (MicroMass, Manchester, UK) equipped with an electro-spray ionization source. Samples (10−20 μL) were injected into solvent flowing at 100 μL/min (70% acetonitrile (aq)/0.1% formic acid (aq)). The orifice potential was set to 90 V and, unless indicated otherwise, spectra were acquired over the mass range 500–2000 amu, with a resolution of 0.1 amu. Reconstructed molecular ions were calculated from the observed m/z values using MassLynx software (MicroMass, Manchester, UK). Masses for PnIA analogues were observed as follows (values in amu): PnIA 1622.93 (calc. 1622.85); [A10L] 1664.60 (calc. 1664.93); [A10Abu] 1637.06 (calc. 1636.88); [A10Nva] 1651.12 (calc. 1650.91); [A10Nle] 1664.68 (calc. 1664.93); [A10V] 1650.86 (calc. 1650.91); [A10I] 1665.63 (calc. 1664.93); [A10M] 1682.82 (calc. 1682.97); [A10Aha] 1678.14 (calc. 1678.63); [A10Aoa]

1691.12 (calc. 1691.25); [A10Cha] 1704.19 (calc. 1703.99); [A10F] 1698.76 (calc. 1698.95); [A10Nal] 1749.52 (calc. 1749.01); [A10S] 1638.96 (calc. 1638.85); [A10D] 1666.48 (calc. 1666.86); [A10E] 1681.07 (calc. 1680.88); [A10K] 1680.38 (calc. 1679.95).

**2.5 Radioligand Displacement Assays**

Radioligand displacement assays were performed on a $P_2$ rat brain membranes, prepared as described previously [37]. Non-specific binding was determined in the presence of 1 μM unlabeled α-bungarotoxin. Ten-fold serial dilutions of the test compounds were made in incubation buffer (50 mM HEPES, 100 mM NaCl, 0.2% BSA, pH 7.4). The test compound (100 μL) was added to a 12 mm x 75 mm polypropylene culture tube along with 100 μL of 3 nM $^{125}$Iα-bungarotoxin (Amersham, Sydney Australia) and 100 μL of the $P_2$ membrane. Compounds were incubated for 1 h. The membrane was collected and washed on Whatman GF/C filters (blocked with incubation buffer) with 3 x 2 mL volumes of ice cold wash buffer (incubation buffer without BSA). Radioactivity was determined by direct counting of the glass filters by a CliniGamma 1272 gamma counter (Wallac, Turku Finland). Results were analyzed using Prism v4.0b (GraphPad Software, Inc., San Diego, CA) and Ki was calculated using the One site – fit Ki function, with the radioligand concentration and Kd constrained to 1 nM. Data were analyzed using 1-way ANOVA analysis with Tukey's test and were considered significantly different when $p < 0.05$.

**2.6 Electrophysiological recordings from exogenously expressed nAChRs in Xenopus oocytes**

RNA preparation, oocyte preparation and expression of nAChR subunits in *Xenopus* oocytes were performed as described previously [38,39]. Briefly, capped RNA was synthesized from

cDNA encoding the rat α7 and α3β2 and human α7 and α4β2 nAChR subunits using an *in vitro* transcription kit (Ambion mMessage mMachine, Austin, TX). cRNA yield was determined by spectrophotometry.

*Xenopus laevis* were anaesthetized using tricaine methanesulfonate (1.3 g/L). Oocytes were surgically removed, then placed in OR2 buffer (82.5 mM NaCl, 2 mM KCl, 1 mM $CaCl_2$, 1 mM $MgCl_2$ and 5 mM HEPES at pH 7.4) with 3 mg/mL collagenase at room temperature for 1–2 h. Collagenase was removed by rinsing 3 times in the same OR2 solution, followed by a further 3 rinses in the final ND96 solution (96 mM NaCl, 2 mM KCl, 1 mM $CaCl_2$, 1 mM $MgCl_2$ and 5 mM HEPES at pH 7.4), supplemented with 50 mg/L gentamycin, 5 mM pyruvic acid and 5% horse serum. Defolliculated oocytes were injected with ~ 5 ng cRNA for each subunit (1:1 subunit ratio for α3β2 and α4β2) in 50 nL volume using a microinjector (Nanoject II™, Drummond Scientific Co., Broomall, PA), then kept at 18°C in the supplemented ND96 solution for 2−7 d before recording.

Membrane currents were recorded from oocytes using the two-electrode (virtual ground circuit) voltage-clamp technique. Oocytes were placed in a bath (~ 200 µL) containing ND96 solution, impaled with glass microelectrodes and voltage-clamped at a holding potential of –80 mV using a GeneClamp 500B amplifier (Molecular Devices, Sunnyvale, CA). Microelectrodes were pulled from borosilicate glass (GC150TF-7.5, Harvard Apparatus, Holliston MA) and had resistances between 0.2 – 1.5 MΩ when filled with 3M KCl. All recordings were conducted at room temperature (22°C). Acetylcholine (100 µM) was applied via a gravity-fed perfusion system for 3 s (at ~ 2 mL/min), with 5 min washout periods between successive applications. α-Ctx [A10L]PnIA analogues were applied directly into the bath and incubated for at least 5 min, before a further application of agonist [23]. Directly adding peptides to the bath conserved

material and avoided any potential adhesion to tubing surfaces. Data were sampled at 1 kHz and filtered at 200 Hz. Peak current amplitude was measured before and after incubation of [A10L]PnIA analogues. Concentration−response curves for peptide inhibition of ACh-evoked peak current amplitude were fitted to the empirical Hill equation. $IC_{50}$ and Hill coefficients ($n^H$) were determined and t-tests were used to determine significance.

**2.7 Computational Modeling and Docking Simulation**

Based on the co-crystal structures of AChBP, no significant backbone movements were observed upon ligand binding, except for C-loop and F-loop located at the interface between the two subunits. Therefore, homology models of α7 and α3ß2-nAChR with open and closed C-loop conformations were created first, using the co-crystal structure of PnIA-*Ac*-AChBP (PDB ID 2BR8) [28] and HEPES-*Ls*-AChBP (PDB ID 1I9B) [25] as described in Jin *et al.* 2008 [39] and Luo *et al.* 2010 [40], respectively. To search for the suitable binding site conformation for each PnIA analogue, 20 intermediate α7 and α3ß2-nAChR conformers with 0.5 Å RMSD between the open and closed C-loop conformation were generated using Morphing server [41]. All homology models were subjected for energy minimization using GROMOS 96 [42], with 500 steps of steepest descent followed by 1,000 cycles of conjugated gradient to remove steric incompatibilities. All models were then evaluated using the online server Verify3D [43] and Ramachandran plots available from the ProFunc [44] database. Each PnIA analogue (except for [A10K], [A10E], [A10D] and [A10Nal]PnIA) was docked to the ensemble of 20 intermediate conformers of α7 and α3ß2 nAChR using HEX 6.1 [45]. The α7 and α3ß2 nAChR binding site conformations with the least minimal energy and ligand binding mode with typical α-Ctx binding [46] were chosen. To optimize the ligand−receptor interactions, each PnIA analogue was then re-docked to the chosen α7 and α3ß2 nAChR conformations using Autodock Vina [47]. All of the

PnIA analogue side chains and the binding site of α7 nAChR were set to be fully rotatable. The center of the docking grid map was set as the center of the ligand binding site, with dimensions of 20 x 20 x 20 Å covering the predicted binding site and searching resolution of 0.375 Å. Solutions with minimal energies less than 5 kcal/mol in difference from the best solution were selected for analysis.

## 3. Results

We designed and synthesized 17 α-Ctx PnIA position 10 analogues. We first tested their ability to compete with radiolabelled α-bungarotoxin (an α7 nAChR-specific ligand) in a rat brain homogenate and then assessed their inhibition of ACh-induced currents in pure populations of recombinant receptors expressed in *Xenopus* oocytes. The analogues contained aliphatic (aminobuteric acid (Abu), norvaline (Nva), norleucine (Nle), valine, isoleucine, methionine, cyclohexylalanine (Cha), aminoheptanoic acid (Aha), and aminooctanoic acid), aromatic (phenylalanine and naphthylalanine (Nal)), polar (serine), or charged amino acid (aspartic acid, glutamic acid and lysine) residues. We synthesized the hydrophobic Aha and aminooctanoic acid from diethyl acetamidomalonate and the corresponding alkyl bromide as described by Blanchfield *et al* [31] **(Figure 1)**.

### 3.1 Radioligand Studies

To evaluate the affinity of each analogue for α7 nAChR, we tested the ability of each to compete with $^{125}$I-α-bungarotoxin in a rat brain homogenate **(Figure 3A and Table 2)**. α-Bungarotoxin

was used because it is known to bind selectively to the α7 nAChR subtype [48].. All analogues displayed Ki values less than 100 μM with the exception of [A10K], [A10E], [A10D] and [A10Nal]PnIA which indicates that extremely bulky or charged residues were not tolerated at position 10.

More specifically, incorporating the small polar residue serine severely reduced affinity more than 7-fold to 2.2 μM. We also observed reduced affinity for isoleucine (Ki 571 nM), Cha (Ki 594 nM), aminooctanoic acid (Ki 756 nM), and Abu (Ki 908 nM). An aromatic side chain reduced affinity for α7 nAChR, with phenylalanine (Ki 1.28 μM), which has a similar shaped side chain as Cha, displaying decreased affinity. α-Ctx PnIA, with an alanine side chain at position 10, had a Ki of 1.03 μM. In contrast, incorporating Nle, which differs from leucine by a one carbon atom extension at the γ carbon atom, at position 10 increased affinity approximately 8-fold more than [A10L]PnIA and gave the lowest Ki observed (44 nM). Small changes to the side chain also improved affinity over [A10L] PnIA (Ki 292 nM), but not significantly. These changes included aminoheptaonic acid (Ki 136 nM), methionine (Ki 132 nM) and valine (Ki 234 nM). Interestingly, removing the γ branch of leucine to give Nva (Ki 327 nM) did not significantly affect affinity.

**3.2 Electrophysiological assays of nAChR subunits expressed in Xenopus oocytes**

We tested α-Ctx PnIA and analogues for their ability to inhibit α7, α3β2 and α4β2 nAChRs expressed in *Xenopus* oocytes. The nAChR subtype selectivity profile was determined first by measuring PnIA and [A10L]PnIA inhibition of ACh-evoked current amplitude at α7 and α3β2 nAChRs, and each analogue at a single concentration (10 nM). α-Ctx PnIA (10 nM) inhibited the ACh-evoked peak current amplitude mediated by α3β2 nAChRs by approximately 65%, whereas

the same concentration inhibited only about 20% of the α7 nAChR-mediated current (data not shown).

To quantify the potency of PnIA and selected analogues, we determined concentration–response relationships, calculated $IC_{50}$ values, and compared the α7 **(Figure 3B)** and α3β2 **(Figure 3C)** nAChR subtypes. Concentration–response curves determined for α-Ctx PnIA inhibition of α7 and α3β2 nAChRs gave $IC_{50}$ values of 62.7 ± 22.9 nM ($n^H$= 1.0) and 7.9 ± 3.7 nM ($n^H$ =0.7), respectively, confirming that PnIA preferentially inhibits α3β2 nAChRs[22,49]. Substituting leucine for alanine at position 10, forming the analogue [A10L]PnIA, substantially reduced potency at α3β2, with an $IC_{50}$ of 369 ± 176 nM ($n^H$=0.8). However, there was no significant change in potency compared with that of PnIA at α7 (50.4 ± 38.8 nM; $n^H$=1.0). The difference in potency of [A10L]PnIA at the two nAChR subtypes indicates a switch in selectivity and that [A10L]PnIA is α7-selective.

The analogue [A10M]PnIA was similar to PnIA, with concentration–response relationships giving $IC_{50}$ values of 52.1 ± 7.2 nM ($n^H$=1.0) and 13.0 ± 0.0 ($n^H$=1.0) nM at the α7 and α3β2 nAChRs, respectively. Although potency slightly increased at α7 with [A10M]PnIA, this analogue remained α3β2-selective. Incorporating Nle at position 10 ([A10Nle]PnIA) significantly increased potency at α7 and α3β2 nAChRs, giving $IC_{50}$ values of 4.3 ± 0.1 nM ($n^H$=1.4) and 0.7 ± 0.5 nM ($n^H$=1.0), respectively. Substituting Aha at position 10 also increased potency at α7 ($IC_{50}$ 9.8 ± 3.2 nM; $n^H$=0.7), but its potency at α3β2 remained relatively unchanged ($IC_{50}$ 11.5 ± 4.6 nM; $n^H$=1.0). This resulted in a lack of selectivity between the nAChR subtypes. Interestingly, recovery of the ACh-evoked current amplitude from inhibition by [A10Aha]PnIA at α7 nAChR to pre-incubation (control) levels took almost 20 min, which

was substantially longer than for the other PnIA analogues. Recovery from block by [A10L]PnIA, [A10M]PnIA and [A10Nle]PnIA occurred within 4 min after peptide washout. All [A10L]PnIA analogues were tested at 150 nM at human α4β2 nAChRs, but did not exhibit any significant difference to PnIA; [A10L]PnIA normalized current value 0.50 ± 0.15 compared to PnIA normalized current value 0.52 ± 0.13 (n = 5). This indicates that activity at human α4β2 receptors was unaffected by changing the properties of the side chain at position 10 of PnIA.

### 3.3 Molecular Docking Studies

Studies have shown that the dominant interaction involved in binding PnIB, a closely related α-conotoxin that differs from [A10L]PnIA by a single amino acid at position 10, to the human α7 nAChR is between Leu-10 and Trp-149 [50]. Our docking simulations showed that the residue at position 10 in all 12 high-affinity α-Ctx PnIA analogues and α-Ctx PnIA interacted with a hydrophobic pocket between the two α7 subunits. This hydrophobic pocket resembles a funnel structure comprising the highly conserved hydrophobic residues Val-130(-), Tyr-140(–), Leu-141(–), Pro-143(–) and Trp-171(+), plus flanking polar residues Thr-128(–) and Ser-172(+) (**Figures 4A–4C**). Our results revealed extensive hydrophobic interactions between the funnel residues Val-130(–), Leu-141(–) and Trp-171(+) and position 10 residues of all 12 PnIA analogues. However, weak hydrophobic and van-der-Waal's interactions were found for PnIA. This suggests that a longer hydrophobic side chain at position 10 of PnIA can increase contacts with this region of the α7 nAChR. This result is consistent with our experimental data, where all 12 analogues have the same binding affinity for α7 nAChR that PnIA does – or higher. It may also explain the large reduction in the affinity of PnIA analogues with charged or polar side chains at position 10.

Closer examination of the docking results indicated that the funnel width accommodates linear and branched side chains, not aromatic chains. This may explain the slightly lower affinity of [A10F]PnIA and [A10Cha]PnIA for the α7 nAChR than PnIA analogues with linear or branched side chains. Structural analysis also suggests that α-Ctx [A10Nal]PnIA loses its binding affinity because the fused aromatic rings are too large for the binding site or funnel. The depth of the funnel is also pivotal in accommodating the position 10 side chains of α-Ctx PnIA analogues. When extended, the side chain length of [A10Aha]PnIA is roughly 5.5Å from the Cα to the tip, with the [A10Nle] side chain a bond shorter. Our α-Ctx [A10Aha]PnIA docking solution shows that this tip extends into the funnel, while the long chain of α-Ctx [A10Aoa]PnIA, with five methylene groups, needs the overall ligand to bind slightly shallower so it can extend its side chain. This may perturb the binding mode for α-Ctx PnIA.

Studies of PnIA, [A10L]PnIA, [A10M]PnIA, [A10Aha]PnIA and [A10Nle]PnIA docking to α3β2 nAChR generated similar outcomes to the α7 nAChR docking studies. Our results showed that the position 10 residue of [A10M]PnIA, [A10Aha]PnIA, [A10Nle]PnIA and PnIA interact with the hydrophobic funnel formed between the α3 and β2 subunit (**Figures 4E and 4F**). This hydrophobic funnel, located at the equivalent position in the α7 nAChR (**Figures 4B and 4C**), is formed by six conserved hydrophobic residues Val-111(–), Phe-119(–), Leu-121(–), Pro-122(–), Pro-123(–) and Trp-149(+).

Docking simulations revealed that linear hydrophobic side chains favorably interact with the α3β2 subtype, consistent with α7 nAChR docking outcomes. Unexpectedly, [A10L]PnIA docked in a different orientation, where the position 10 residue interacts with the hydrophobic patch (Ile-186, Tyr-188, Try-195) on the C-loop of α3 subunit (**Figure 4D**). Interestingly, the corresponding

hydrophobic patch residues in α7 nAChR are Arg-208, Tyr-210 and Tyr-217, respectively. This suggests that the residue at position 208 in α7 (186 in α3) plays a role in accommodating branched and bulky side chain residues from linear side chain residues at position 10. This is in agreement with the recently published mutational studies on α3β2 and α4β2 nAChR, which demonstrated that α3[I186R]β2 impairs binding of α-conotoxins MII, TxIA and [A10L]TxIA, while the α4[R185I]β2 mutant enhances binding[51] In addition, a structural comparison between ACh binding pockets of α7 and α3β2 nAChRs showed that the entrance of the hydrophobic funnel in the α3β2 nAChR is narrower than that of the α7 nAChR funnel, increasing the likelihood of steric clashes with branched side chain residues. A significantly altered [A10L]PnIA binding mode at α3β2 nAChRs provides a plausible explanation for the significant reduced affinity of [A10L]PnIA for the α3β2 nAChR.

## 4. Discussion

Compounds that bind potently and selectively to distinct subtypes of ion channels and receptors have great potential as pharmacological probes and drug leads [13,14,16,18]. Neuronal nAChRs are a diverse class of ligand-gated ion channels involved in neurological conditions such as neuropathic pain [52,53] and Alzheimer's disease [54,55]. Therefore, a suite of potent and selective ligands would be an invaluable pharmacological tool to identify the physiological role of nAChR subunit combinations.

α-Ctx discovery in conjunction with chemical peptide synthesis has provided an increasing array of biologically active compounds with varying subtype selectivity [13,14,16-23,56]. Based on the observation that the residue at position 10 of the 4/7 class of α-Ctxs can influence nAChR

subtype selectivity between α7 and α3β2 nAChRs, we initially investigated the effects of coded and non-coded position 10 mutants of varying shape, size and polarity on α-Ctx PnIA analogue affinity for the α7 nAChR. Each analogue was synthesized in good yield and tested for its ability to compete with radiolabelled α-bungarotoxin for the α7 nAChR in a rat brain homogenate **(Figure 3A and Table 2).** We also tested all analogues for inhibition of ACh-induced currents in a pure population of receptors expressed in *Xenopus* oocytes, to evaluate their functional activity (**Figures 3B and 3C**).

Modest molecular changes to the side chain at position 10 significantly changed receptor affinity. Based on sequence identity between the 4/7 α-conotoxins at position 10 **(Table 1)**, mutations were made to hydrophobic residues with different structural characters – focusing on linear or beta-branched aliphatic, or aromatic ring-containing residues. We compared the changes in the affinity of these analogues with α-Ctx [A10L]PnIA, because the introduction of a branched aliphatic residue at position 10 was previously reported [20-22,56] to be responsible for the switch in subtype selectivity from α3β2 to α7. In our binding assay, α-Ctx [A10L]PnIA had 4-fold higher affinity for α7 nAChR than did PnIA, with Ki values of 292 nM and 1.03 μM, respectively. To confirm the need for hydrophobicity at position 10, we included analogues that incorporated lysine, aspartic acid and glutamic acid. As expected, incorporating a charged residue at position 10 severely affected affinity, decreasing it to > 100 μM. This was 50-fold less than α-Ctx PnIA and almost 150-fold less than the α7-selective analogue α-Ctx [A10L]PnIA. Incorporating the bulky aromatic Nal side chain also disrupted binding, with its $IC_{50}$ values increasing to > 100 μM.

All other analogues maintained significant though varying levels of affinity for the α7 nAChR. Of particular interest was a series of analogues for which the side chain at position 10 was increased one carbon−carbon bond length at a time, from 1 (alanine) through 6 (aminooctanoic acid) **(Figure 1)**. Lengthening the side chain stepwise from alanine to Abu to Nva, also restored affinity in steps, from PnIA back to the level seen for [A10L]PnIA. Rearranging the side chain from Nva to valine slightly increased affinity. However, lengthening the side chain by one carbon-carbon bond, from Nva to Nle, dramatically improved affinity by 7.5-fold, considering the conservative nature of the change with α-Ctx [A10Nle]PnIA having the highest affinity for α7 nAChR, with Ki 44 nM. Extending the side chain past Nle to Aha and aminooctanoic acid decreased affinity to 136 nM and 756 nM, respectively.

Any change to the hydrophobicity of the position 10 residue always decreased affinity. This was evident when comparing Abu with serine, and Nle with methionine. Each pair of side chains were of similar size and polarity except for the hydroxyl group of serine, which decreased the affinity of Abu from 908 nM to 2.2 μM, and the sulfur atom in the methionine, which reduced Nle's affinity from 44 nM to 132 nM. Although the phenylalanine analogue's affinity was much higher than that of Nal, its affinity was approximately 50% weaker than that of Cha. This indicates that the binding environment prefers hydrophobic side chains to aromatic ones.

Electrophysiology experiments demonstrated that [A10L]PnIA and PnIA retained the greatest functional selectivity for the α7 and α3β2 subtypes, respectively. In agreement with the binding data, the α-Ctx [A10Nle]PnIA potency also greatly increased, though unlike α-Ctx [A10L]PnIA, selectivity reverted from α7 to α3β2. In contrast to the leucine-alanine selectivity switch, the leucine-Nle switch in selectivity demonstrates the importance of subtle changes in the position 10

side chain, where the exact placement of a single methyl group determines selectivity. Any further increase in the side chain size eliminated selectivity between the two receptor subtypes, while maintaining low nanomolar potency. These results indicate it is primarily the size and shape of the side chain, not its chemical properties, that determine selectivity.

The versatility of chemical peptide synthesis has enabled us to employ coded and non-coded amino acids to explore different side chains at position 10 of PnIA. This has greatly expanded the diversity of side chain space explored. Our findings suggest that Nle is the ideal length of the side chain at position 10 for improved affinity for the α7 nAChR subtype. Importantly, computational studies provide a molecular basis for ligand selectivity between α7 and α3β2 nAChRs, where the residue located at the equivalent position to Arg 208 in α7 (equivalent to Ile 186 in α3) is one of the key determinants for ligand selectivity. Structurally, it appears that a highly conserved hydrophobic funnel in these nAChRs accommodates residues with a longer and more hydrophobic linear or branched side chain than alanine. The high similarity between our computational and experimental data indicates that hydrophobicity of the position 10 residue in α-Ctx PnIA is critical for its recognition of the α7 and α3β2 nAChRs. Our finding that a single methyl group is needed for subtype selectivity may be useful in the design of selective peptides that distinguish between α7 and α3β2 nAChRs.

**Acknowledgements**

We thank Ms Lucy Corke for assisting with the electrophysiological assays. This work was support by an Australian Research Council (ARC) Discovery Grant (DJA, PFA, RJL). DJA is an

ARC Australian Professorial Fellow, RJL is a National Health and Medical Research Council Research Fellow.

**References**


[1] Macdonald RL, Olsen RW. $GABA_A$ receptor channels. Annu Rev Neurosci 1994;17:569–602.

[2] Jackson MB, Yakel JL. The 5-$HT_3$ receptor channel. Annu Rev Physiol 1995;57:447–68.

[3] Lynch JW. Molecular structure and function of the glycine receptor chloride channel. Physiol Rev 2004;84:1051–95.

[4] Clementi F, Fornasari D, Gotti C. Neuronal Nicotinic Receptors. New York: Springer; 2000.

[5] Arnerić S, Brioni JD, editors. Neuronal nicotinic receptors: pharmacology and therapeutic opportunities. New York: Wiley; 1999.

[6] Itier V, Bertrand D. Neuronal nicotinic receptors: from protein structure to function. FEBS Letters 2001;504:118–25.

[7] Jones S, Sudweeks S, Yakel JL. Nicotinic receptors in the brain: correlating physiology with function. Trends Neurosci 1999;22:555–61.

[8] Dani JA. Overview of nicotinic receptors and their roles in the central nervous system. Biol Psychiatry 2001;49:166–74.

[9] Ripoll N, Bronnec M, Bourin M. Nicotinic receptors and schizophrenia. Curr Med Res Opin 2004;20:1057–74.

[10] Di Corcia G, Blasetti A, De Simone M, Verotti A, Chiarelli F. Recent advances on autosomal dominant nocturnal frontal lobe epilepsy: understanding the nicotinic acetylcholine receptor (nAChR). Eur J Paed Neur 2005;9:59–66.

[11] Wang H, Yu M, Ochani M, Amella CA, Tanovic M, Susarla S, et al. Nicotinic acetylcholine receptor α7 subunit is an essential regulator of inflammation. Nature 2003;421:384–8.

[12] Guyon T, Wakkach A, Poea S, Mouly V, Klingel-Schmitt I, Levasseur P, et al. Regulation of acetylcholine receptor gene expression in human myasthenia gravis muscles. Evidences for a compensatory mechanism triggered by receptor loss. J Clin Invest 1998;102:249–63.

[13] Azam L, McIntosh JM. α-conotoxins as pharmacological probes of nicotinic acetylcholine receptors. Acta Pharmacol Sin 2009;30:771–83.

[14] Halai R, Craik DJ. Conotoxins: natural product drug leads. Nat Prod Rep 2009;26:526–36.

[15] Hone AJ, Whiteaker P, Christensen S, Xiao Y, Meyer EL, McIntosh JM. A novel fluorescent α-conotoxin for the study of α7 nicotinic acetylcholine receptors. J Neurochem 2009;111:80–9.

[16] Lewis RJ. Conotoxin venom peptide therapeutics. Adv Exp Med Biol 2009;655:44–8.

[17] Arias HR, Blanton MP. Alpha-conotoxins. Int J Biochem Cell Biol 2000;32:1017–28.

[18] Dutton JL, Craik DJ. α-Conotoxins: nicotinic acetylcholine receptor antagonists as pharmacological tools and potential drug leads. Curr Med Chem 2001;8:327–44.

[19] Millard EL, Daly NL, Craik DJ. Structure-activity relationships of α-conotoxins targeting neuronal nicotinic acetylcholine receptors. Eur J Biochem 2004;271:2320–6.

[20] Broxton N, Miranda L, Gehrmann J, Down J, Alewood PF, Livett B. Leu(10) of α-conotoxin PnIB confers potency for neuronal nicotinic responses in bovine chromaffin cells. Eur J Pharmacol 2000;390:229–36.

[21] Hogg RC, Miranda LP, Craik DJ, Lewis RJ, Alewood PF, Adams DJ. Single amino acid

substitutions in α-conotoxin PnIA shift selectivity for subtypes of the mammalian neuronal nicotinic acetylcholine receptor. J Biol Chem 1999;274:36559–64.

[22] Luo S, Nguyen TA, Cartier GE, Olivera BM, Yoshikami D, McIntosh JM. Single-residue alteration in α-conotoxin PnIA switches its nAChR subtype selectivity. Biochemistry 1999;38:14542–8.

[23] Hogg RC, Hopping G, Alewood PF, Adams DJ, Bertrand D. Alpha-conotoxins PnIA and [A10L]PnIA stabilize different states of the alpha7-L247T nicotinic acetylcholine receptor. J Biol Chem 2003;278:26908–14.

[24] Dutertre S, Nicke A, Tyndall JDA, Lewis RJ. Determination of α-conotoxin binding modes on neuronal nicotinic acetylcholine receptors. J Mol Recognit 2004;17:339–47.

[25] Brejc K, van Dijk WJ, Klaassen RV, Schuurmans M, van Der Oost J, Smit AB, et al. Crystal structure of an ACh-binding protein reveals the ligand-binding domain of nicotinic receptors. Nature 2001;411:269–76.

[26] Celie PHN, Klaassen RV, van Rossum-Fikkert SE, van Elk R, van Nierop P, Smit AB, et al. Crystal structure of acetylcholine-binding protein from *Bulinus truncatus* reveals the conserved structural scaffold and sites of variation in nicotinic acetylcholine receptors. J Biol Chem 2005;280:26457–66.

[27] Celie P, van Rossum-Fikkert S, Van Dijk W. Nicotine and carbamylcholine binding to nicotinic acetylcholine receptors as studied in AChBP crystal structures. Neuron 2004;41:907–14.

[28] Celie PHN, Kasheverov IE, Mordvintsev DY, Hogg RC, van Nierop P, van Elk R, et al. Crystal structure of nicotinic acetylcholine receptor homolog AChBP in complex with an α-conotoxin PnIA variant. Nat Struct Mol Biol 2005;12:582–8.

[29] Dutertre S, Ulens C, Büttner R, Fish A, van Elk R, Kendel Y, et al. AChBP-targeted α-conotoxin correlates distinct binding orientations with nAChR subtype selectivity. EMBO J 2007;26:3858–67.

[30] Ulens C, Hogg RC, Celie PH, Bertrand D, Tsetlin V, Smit AB, et al. Structural determinants of selective α-conotoxin binding to a nicotinic acetylcholine receptor homolog AChBP. Proc Natl Acad Sci USA 2006;103:3615–20.

[31] Blanchfield JT, Dutton JL, Hogg RC, Gallagher OP, Craik DJ, Jones A, et al. Synthesis, structure elucidation, in vitro biological activity, toxicity, and Caco-2 cell permeability of lipophilic analogues of α-conotoxin MII. J Med Chem 2003;46:1266–72.

[32] Schnölzer M, Alewood PF, Jones A, Alewood D, Kent SBH. In situ neutralization in Boc-chemistry solid phase peptide synthesis. Rapid, high yield assembly of difficult sequences. Int J Pept Protein Res 1992;40:180–93.

[33] Sarin VK, Kent SBH, Tam JP, Merrifield RB. Quantitative monitoring of solid-phase peptide synthesis by the ninhydrin reaction. Analytical Biochemistry 1981;117:147–57.

[34] Dutton JL, Bansal PS, Hogg RC, Adams DJ, Alewood PF, Craik DJ. A new level of conotoxin diversity, a non-native disulfide bond connectivity in α-conotoxin AuIB reduces structural definition but increases biological activity. J Biol Chem 2002;277:48849–57.

[35] Gehrmann J. Structure/Function Studies of the α-Conotoxin Disulfide Bond Framework. University of Queensland, n.d. year?

[36] Nielsen JS, Buczek P, Bulaj G. Cosolvent-assisted oxidative folding of a bicyclic α-conotoxin ImI. J Pept Sci 2004;10:249–56.

[37] Rapier C, Lunt GG, Wonnacott S. Nicotinic modulation of [$^3$H]dopamine release from striatal synaptosomes: pharmacological characterisation. J Neurochem 1990;54:937–45.
[38] Clark RJ, Fischer H, Nevin ST, Adams DJ, Craik DJ. The synthesis, structural characterization, and receptor specificity of the α-conotoxin Vc1.1. J Biol Chem 2006;281:23254–63.
[39] Jin A-H, Daly NL, Nevin ST, Wang C-IA, Dutertre S, Lewis RJ, et al. Molecular engineering of conotoxins: the importance of loop size to α-conotoxin structure and function. J Med Chem 2008;51:5575–84.
[40] Luo S, Akondi KB, Zhangsun D, Wu Y, Zhu X, Hu Y, et al. Atypical α-conotoxin LtIA from *Conus litteratus* targets a novel microsite of the α3β2 nicotinic receptor. J Biol Chem 2010;285:12355–66.
[41] Krebs WG, Gerstein M. The morph server: a standardized system for analyzing and visualizing macromolecular motions in a database framework. Nucleic Acids Res 2000;28:1665–75.
[42] van Gunsteren W, Berendsen H. Computer simulation of molecular dynamics: Methodology, applications, and perspectives in chemistry. Angew Chem Int Ed Engl 1990;29:992–1023.
[43] Bowie JU, Lüthy R, Eisenberg DS. A method to identify protein sequences that fold into a known three-dimensional structure. Science 1991;253:164–70.
[44] Laskowski RA, Watson JD, Thornton JM. ProFunc: a server for predicting protein function from 3D structure. Nucleic Acids Res 2005;33:W89–93.
[45] Ritchie DW, Kemp GJ. Protein docking using spherical polar Fourier correlations. Proteins: Structure, Function, and Bioinformatics 2000;39:178–94.
[46] Hansen SB, Sulzenbacher G, Huxford T, Marchot P, Taylor P, Bourne Y. Structures of Aplysia AChBP complexes with nicotinic agonists and antagonists reveal distinctive binding interfaces and conformations. EMBO J 2005;24:3635–46.
[47] Trott O, Olson A. AutoDock Vina: improving the speed and accuracy of docking with a new scoring function, efficient optimization, and multithreading. J Comput Chem 2010;31:455–61.
[48] Drisdel RC, Green WN. Neuronal alpha-bungarotoxin receptors are alpha7 subunit homomers. Journal of Neuroscience 2000;20:133–9.
[49] Everhart D, Reiller E, Mirzoian A, McIntosh JM, Malhotra A, Luetje CW. Identification of residues that confer α-conotoxin-PnIA sensitivity on the α3 subunit of neuronal nicotinic acetylcholine receptors. J Pharmacol Exp Ther 2003;306:664–70.
[50] Quiram PA, McIntosh JM, Sine SM. Pairwise interactions between neuronal alpha(7) acetylcholine receptors and α-conotoxin PnIB. J Biol Chem 2000;275:4889–96.
[51] Beissner M, Dutertre S, Schemm R, Danker T, Sporning A, Grubmüller H, et al. Efficient binding of 4/7 α-conotoxins to nicotinic α4β2 receptors is prevented by Arg185 and Pro195 in the α4 subunit. Mol Pharmacol 2012;82:711–8.
[52] Bannon AW, Decker MW, Kim DJ, Campbell JE, Arneric SP. ABT-594, a novel cholinergic channel modulator, is efficacious in nerve ligation and diabetic neuropathy models of neuropathic pain. Brain Res 1998;801:158–63.
[53] Vincler M, Wittenauer S, Parker R, Ellison M, Olivera BM, McIntosh JM. Molecular mechanism for analgesia involving specific antagonism of α9α10 nicotinic acetylcholine receptors. Proc Natl Acad Sci USA 2006;103:17880–4.
[54] Whitehouse PJ, Martino AM, Antuono PG, Lowenstein PR, Coyle JT, Price DL, et al.

Nicotinic acetylcholine binding sites in Alzheimer's disease. Brain Res 1986;371:146–51.

[55] Lilja AM, Porras O, Storelli E, Nordberg A, Marutle A. Functional interactions of fibrillar and oligomeric amyloid-β with α7 nicotinic receptors in Alzheimer's disease. J Alzheimers Dis 2011;23:335–47.

[56] Broxton N, Down J, Miranda L, Alewood PF. Two amino acid residues in α-conotoxins PnIA and PnIB confer potency for the neuronal nicotinic response. Proc Aust Neurosci Soc 1998;9:128.

[57] Fainzilber M, Hasson A, Oren R, Burlingame AL, Gordon D, Spira ME, et al. New mollusc-specific α-conotoxins block *Aplysia* neuronal acetylcholine receptors. Biochemistry 1994;33:9523–9.

[58] Loughnan M, Bond T, Atkins A, Cuevas J, Adams DJ, Broxton NM, et al. α-conotoxin EpI, a novel sulfated peptide from *Conus episcopatus* that selectively targets neuronal nicotinic acetylcholine receptors. J Biol Chem 1998;273:15667–74.

[59] Nicke A, Samochocki M, Loughnan ML, Bansal PS, Maelicke A, Lewis RJ. Alpha-conotoxins EpI and AuIB switch subtype selectivity and activity in native versus recombinant nicotinic acetylcholine receptors. FEBS Lett 2003;554:219–23.

[60] Nicke A, Loughnan ML, Millard EL, Alewood PF, Adams DJ, Daly NL, et al. Isolation, structure, and activity of GID, a novel α 4/7-conotoxin with an extended N-terminal sequence. J Biol Chem 2003;278:3137–44.

[61] Lang PM, Burgstahler R, Haberberger RV, Sippel W, Grafe P. A conus peptide blocks nicotinic receptors of unmyelinated axons in human nerves. Neuroreport 2005;16:479–83.

[62] Cartier GE, Yoshikami D, Gray WR, Luo S, Olivera BM, McIntosh JM. A new α-conotoxin which targets α3β2 nicotinic acetylcholine receptors. J Biol Chem 1996;271:7522–8.

**Figures**

**Figure 1.** Side chain representations of amino acids used in this study. All side chains begin at the α-carbon. Single and triple letter codes are given for coded and non-coded amino acids, respectively.

**Figure 2**. Representative synthetic strategy used to synthesize all 17 peptides. The purified reduced peptide was subject to aerial oxidation for 24 h before further purification. The major product in all cases had the correct 'globular' disulfide connectivity.

**Figure 3.** Concentration−response relationships for α-Ctx PnIA and selected PnIA analogues at the α7 nAChR in a radioligand binding assay, and α7 and α3β2 nAChRs expressed in *Xenopus* oocytes. (**A**) Displacement of $^{125}$Iα-bungarotoxin (1 nM) is plotted as a normalized function of increasing peptide concentration. Response to ACh (100 μM) in the absence and presence of the peptide is plotted as normalized current amplitude for α7 (**B**), and α3β2 (**C**) nAChR subtypes as a function of peptide concentration. Data points represent mean ± SD ($n \geq 3$).

**Figure 4**. Docking simulation of PnIA analogues to α7 and α3β2 nAChR homology models, with position 10 residue in stick and hydrophobic residues in the funnel in orange. (A) Superimposition of all PnIA analogues (except for [A10K]PnIA, [A10D]PnIA, [A10E]PnIA, [A10Nal]PnIA) and PnIA docking to α7 nAChR, with position 10 residues pointing towards the conserved hydrophobic funnel between the two subunits. (B) Surface view of PnIA analogues

showing the hydrophobic funnel. The surface was cropped for clarity. (C) Dissection view of PnIA analogues docking to α7 nAChR, showing the width and depth of the hydrophobic funnel. (D) Molecular surface complementarity of Leu-10 on [A10L]PnIA (green) to C-loop of α3 subunit. Only the interface surface is shown for clarity. (E) Surface view of PnIA, [A10M]PnIA, [A10Aha]PnIA and [A10Nle]PnIA docking to α3β2 nAChR, showing a similar binding mode to that observed for α7 nAChR (B). (F) Dissection view of PnIA, [A10M]PnIA, [A10Aha]PnIA and [A10Nle]PnIA in α3β2 nAChR, showing the relative width and depth of the hydrophobic funnel.

**Table 1.** Sequence and subtype selectivity of some 4/7 α-conotoxins. The residue at position 10 is shown in bold. All peptides are C-terminally amidated. All cysteines are disulfide-bonded in the globular 1-3, 2-4 arrangement. All selectivities are reported for recombinantly expressed receptors, except where indicated (*native tissues).

| Conotoxin | Sequence[#] | Selectivity | Reference |
|---|---|---|---|
| PnIA | GCCSLPPCA**A**NNPDYC | α3β2 > α7 | [57] |
| PnIB | GCCSLPPCA**L**SNPDYC | α7 > α3β2 | [57] |
| [A10L] PnIA | GCCSLPPCA**L**NNPDYC | α7 > α3β2 | [20-23,56] |
| EpI | GCCSDPRCN**M**NNPDYC | α3β2* / α7 | [58,59] |
| GID | IRDECCSNPACR**V**NNPHVC | α7 ≅ α3β2 | [60] |
| Vc1.1 | GCCSDPRCN**Y**DHPEIC | α3β2 > α7 | [61] |
| MII | GCCSNPVCH**L**EHSNLC | α6β2 ≅ α3β2 | [62] |

**Table 2. Results of $^{125}$Iα-Bungarotoxin displacement by additional α-Ctx PnIA analogues**. Each position 10 analogue is indicated by its one or three letter amino acid code. Affinity is presented as Ki ± SD in nM; n*H*, Hill coefficient; n = 3-5 experiments.

| | Radioligand binding | |
|---|---|---|
| **Peptide** | **α7 ($K_i$ nM)** | ***nH*** |
| V | 234 ± 72 | –1.2 |
| Nva | 327 ± 167 | –0.9 |
| I | 571 ± 142 | –1.0 |
| Cha | 594 ± 188 | –0.8 |
| Aoa | 756 ± 226 | –0.9 |
| Abu | 908 ± 412 | –1.0 |
| F | 1,280 ± 466 | –0.6 |
| S | 2,200 ± 795 | –0.8 |

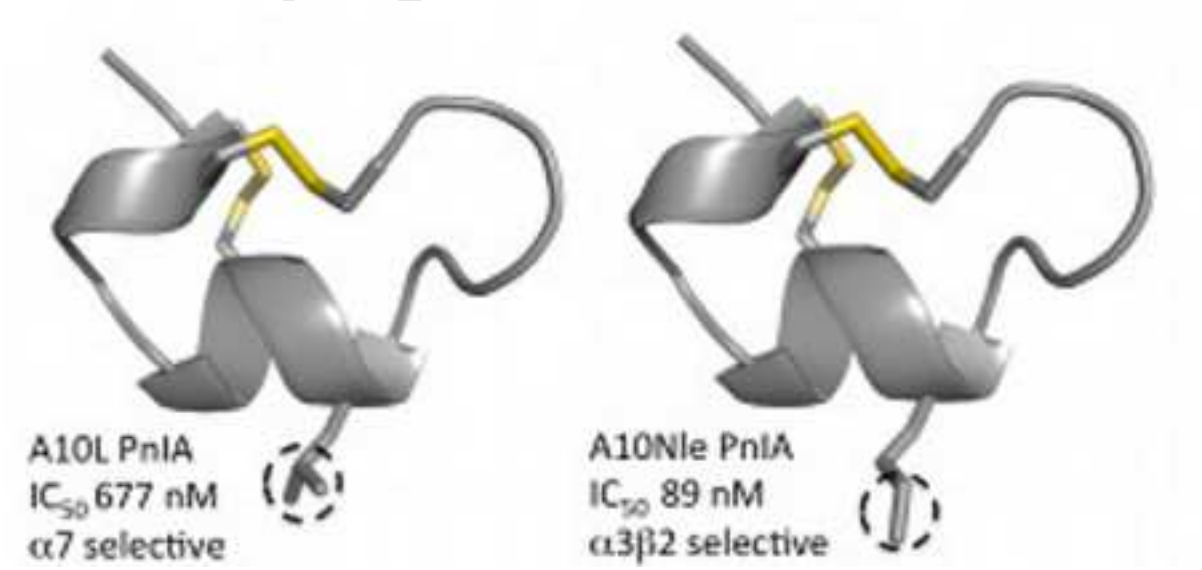
A10L PnIA
IC50 677 nM
α7 selective
A10Nle PnIA
IC50 89 nM
α3β2 selective

**Figure 1**

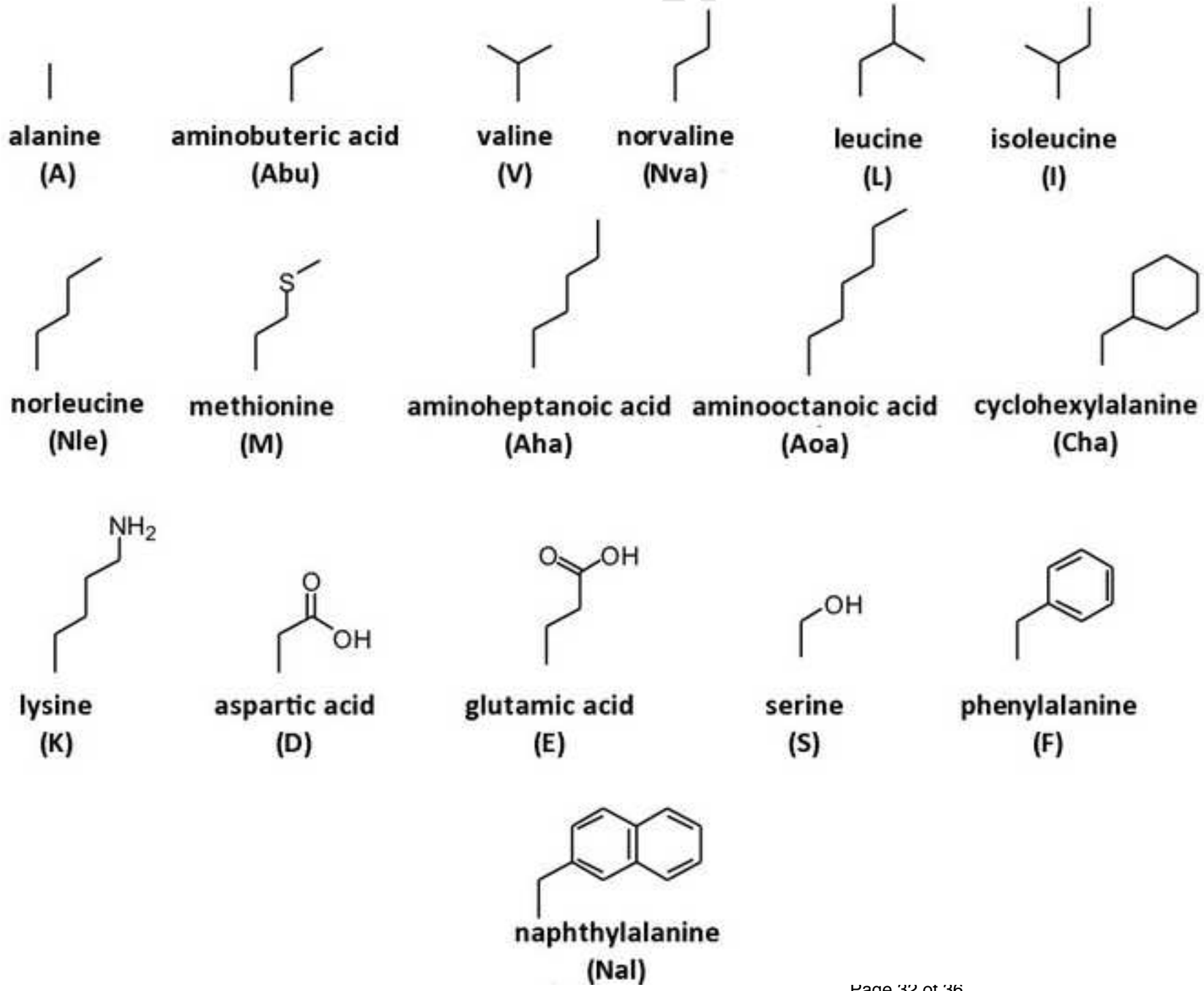
alanine
(A)
aminobuteric acid
(Abu)
valine
(V)
norvaline
(Nva)
leucine
(L)
isoleucine
(I)
norleucine
(Nle)
S
methionine
(M)
aminoheptanoic acid
(Aha)
aminooctanoic acid
(Aoa)
cyclohexylalanine
(Cha)
NH2
lysine
(K)
O
OH
aspartic acid
(D)
O
OH
glutamic acid
(E)
OH
serine
(S)
phenylalanine
(F)
naphthylalanine
(Nal)

**Figure 2**

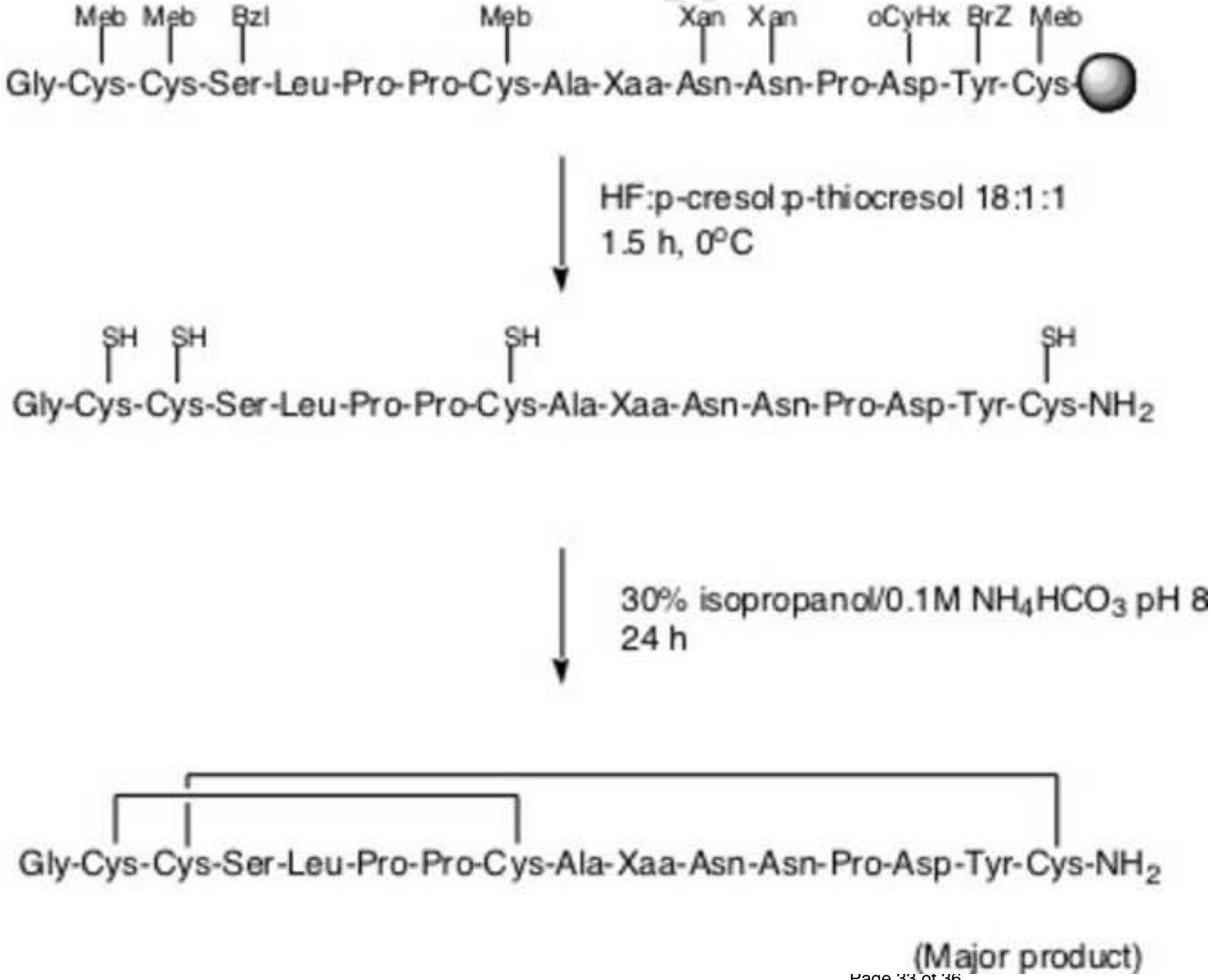
Meb Meb Bzl Meb Xan Xan oCyHx BrZ Meb
Gly-Cys-Cys-Ser-Leu-Pro-Pro-Cys-Ala-Xaa-Asn-Asn-Pro-Asp-Tyr-Cys-
HF:p-cresol:p-thiocresol 18:1:1
1.5 h, 0°C
SH SH SH SH
Gly-Cys-Cys-Ser-Leu-Pro-Pro-Cys-Ala-Xaa-Asn-Asn-Pro-Asp-Tyr-Cys-NH2
30% isopropanol/0.1M NH4HCO3 pH 8
24 h
Gly-Cys-Cys-Ser-Leu-Pro-Pro-Cys-Ala-Xaa-Asn-Asn-Pro-Asp-Tyr-Cys-NH2
(Major product)

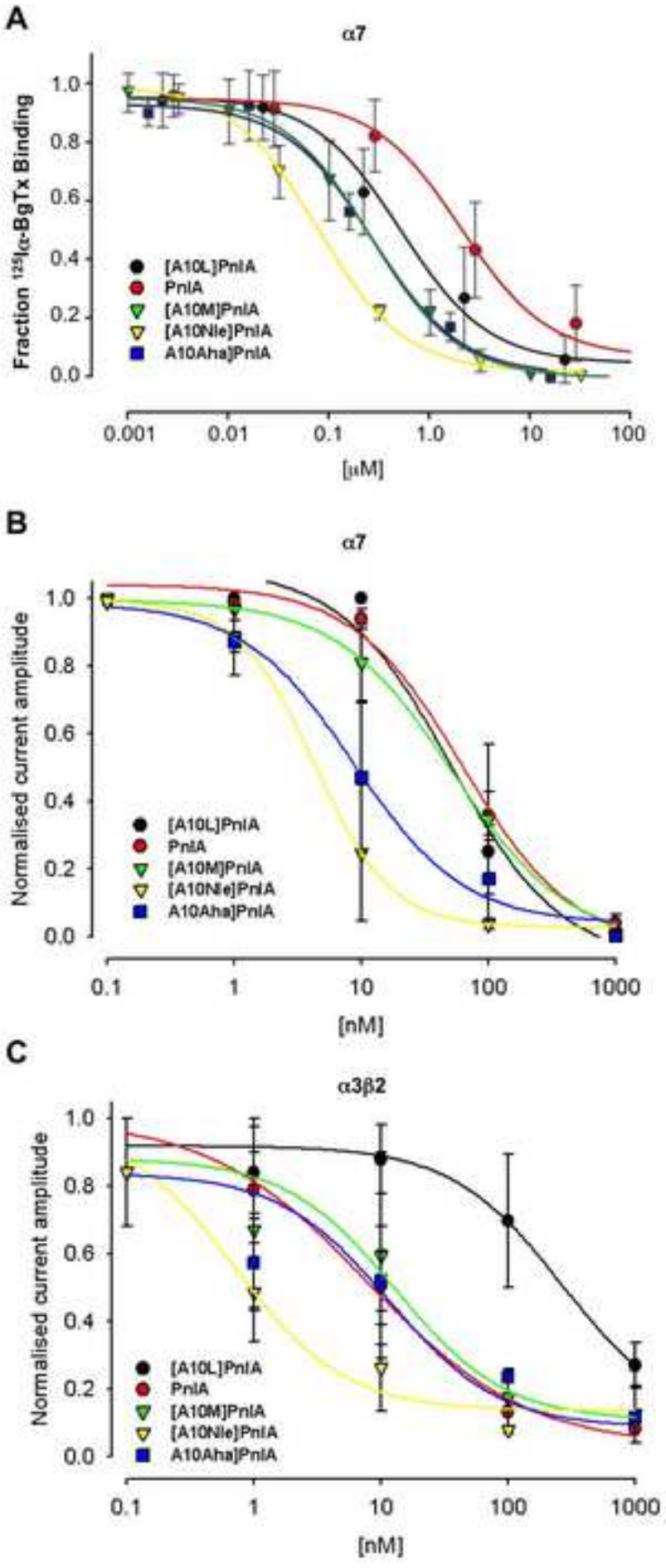

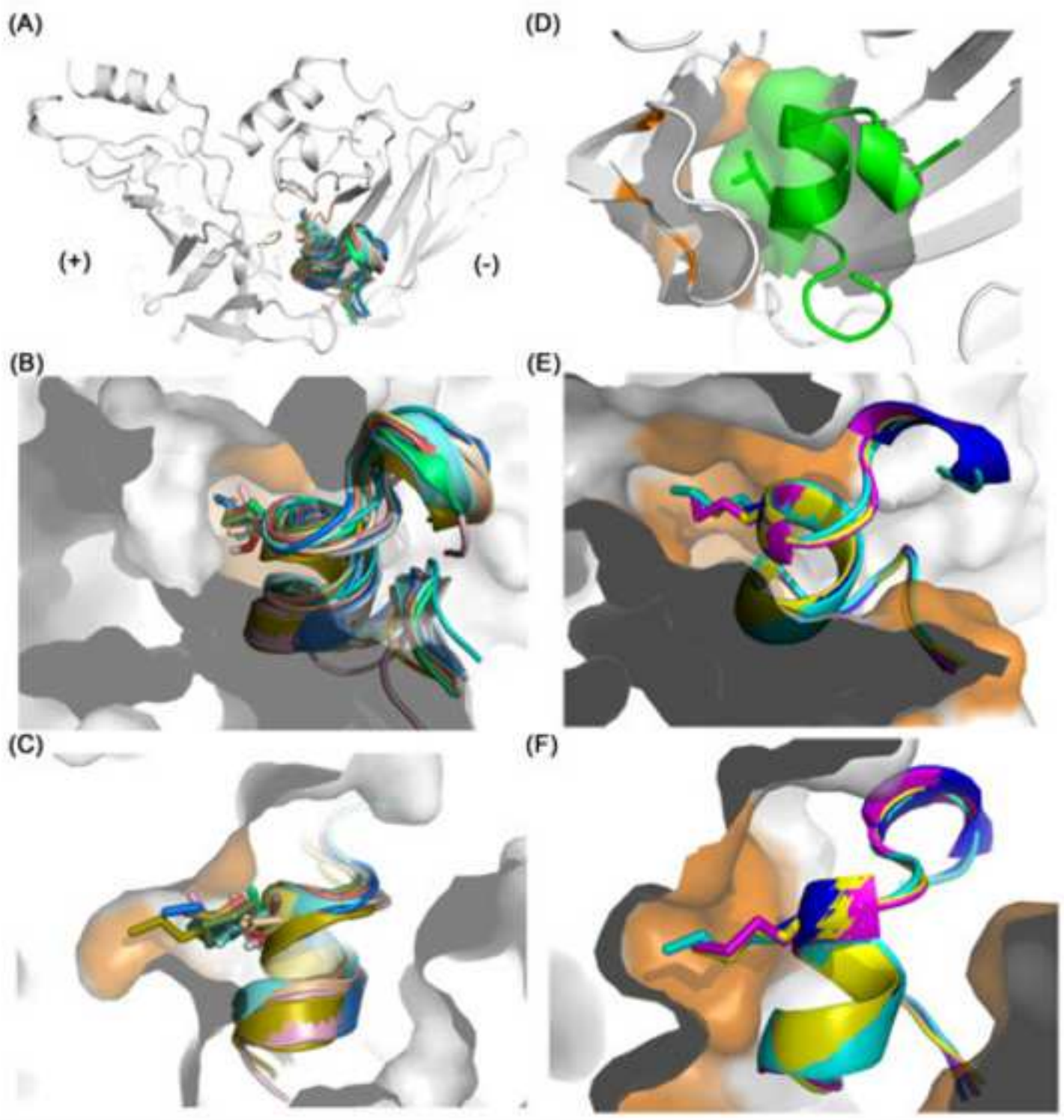

*Graphical Abstract (for review)